BIOCHEMISTRY
including biophysical chemistry & molecular biology

Article

pubs.acs.org/biochemistry

3-Phosphoglycerate Is an Allosteric Activator of Pyruvate Kinase from the Hyperthermophilic Archaeon *Pyrobaculum aerophilum*

J. T. Graham Solomons,[†,§] Ulrike Johnsen,[‡] Peter Schönheit,*[,‡] and Christopher Davies*[,†]

[†]Department of Biochemistry and Molecular Biology, Medical University of South Carolina, Charleston, South Carolina 29425, United States

[‡]Institut für Allgemeine Mikrobiologie, Christian-Albrechts Universität Kiel, Am Botanischen Garten 1-9, Kiel, Germany

Supporting Information

ABSTRACT: Pyruvate kinase (PK) is a highly regulated enzyme that catalyzes the final step of glycolysis. PK from the hyperthermophilic archaeon *Pyrobaculum aerophilum* (*Pa*PK) is distinguished from most PK enzymes of eukarya and bacteria by not responding to any known allosteric effectors and apparently exhibiting only cooperative regulation. We determined the crystal structure of *Pa*PK to 2.2 Å resolution and, in a manner consistent with the lack of a response to conventional effectors, observed that the canonical allosteric site is occluded by a tyrosine. Unexpectedly, though, a bound sulfate was observed at a position equivalent to the 6′-phosphate of sugar effectors, suggesting an allosteric site, but for an unknown effector and sharing only the phosphate position. A search of three-carbon intermediates of glycolysis revealed 3-phosphoglycerate (3PG) as a potent allosteric activator of *Pa*PK. The response was abolished by mutation of residues that contact the sulfate and of an arginine proposed to interact with the 3PG carboxylate group. Regulation of PK by 3PG is consistent with the ancestral glycolysis of hyperthermophilic archaea in which this intermediate is produced by an irreversible enzyme, glyceraldehyde 3-phosphate ferredoxin oxidoreductase. Coordinated regulation within the lower half of glycolysis contrasts sharply with conventional glycolysis in which 3PG is produced reversibly and PK is regulated by fructose 1,6-bisphosphate, the product of phosphofructokinase, an irreversible enzyme in the upper half of the pathway. Regulation of *Pa*PK by a carboxylate molecule rather than a sugar phosphate may reflect a step in the evolution of glycolysis that predates the dominance of sugars in metabolism.

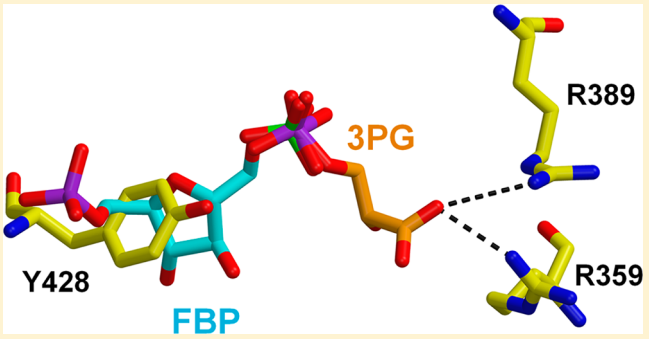

Pyruvate kinase (PK, ATP:pyruvate 2-*O*-phosphotransferase, EC 2.7.1.40) catalyzes the final step of glycolysis, the transfer of a phosphoryl group from phosphoenolpyruvate (PEP) to ADP, producing pyruvate and ATP. Typically, the enzyme exists as a tetramer of identical subunits, in which each subunit consists of three domains (A, B, and C). PK from eukaryotes contains an additional N domain of approximately 40 residues at the N-terminus. As a key energy-producing step and because pyruvate is an important building block for several pathways, this reaction is of central importance for sugar metabolism. Accordingly, the activity of PK is governed by several mechanisms.[1] Most PKs require monovalent[2] and divalent cations[3,4] for activity and display sigmoidal kinetics with respect to the PEP substrate.[5] In addition, most PKs are allosterically activated by sugar phosphates. The most common of these is fructose 1,6-bisphosphate (FBP), but other PKs use ribose 5-phosphate (R5P), fructose 2,6-bisphosphate (F-2,6-BP), or glucose 6-phosphate.[6−12] The binding site for these effectors is located in the C domain near the C−C interface of the tetramer.[13,14] AMP is an allosteric activator of several PKs,[10,15,16] and given that it shares characteristics of sugar phosphates (i.e., it contains both ribose and phosphate moieties), it is assumed to bind to the same canonical allosteric site. A further level of control is exerted in mammals by tissue-specific expression of isoforms of PK with different enzymatic properties.[5,17,18] One of these, the allosteric M2 form, has attracted significant attention as a possible enactor in the so-called Warburg effect.[19] The M2 form differs from its nonallosteric M1 variant in only one differentially spliced exon[20] that corresponds to a segment of the protein that connects the A and C domains of the enzyme. The liver (L) isoform is also regulated by phosphorylation, with the site of phosphorylation being a serine in the small N domain.[21]

Hyperthermophilic archaea are considered among the most ancestral organisms, and their metabolism exhibits several unique features that might reflect earlier stages in evolution.[22] The hyperthermophilic crenarchaeon *Pyrobaculum aerophilum*[23] utilizes a modified Embden−Meyerhof (EM) glycolytic pathway in which several enzymes exhibit novel properties compared to those of their eubacterial or eukaryotic counter-

Received: June 13, 2013
Revised: July 22, 2013
Published: July 23, 2013

   dx.doi.org/10.1021/bi400761b | *Biochemistry* 2013, 52, 5865−5875

parts.[24,25] One of these is pyruvate kinase (*Pa*PK). The distinguishing feature of this enzyme is that, although it exhibits cooperativity for its substrate PEP, *Pa*PK does not respond to any of the classic allosteric effectors of PK.[16] This same is also true of PK from *Aeropyrum pernix*,[16] and *Thermoproteus tenax*,[26] *Sulfolobus solfataricus* (U. Johnsen and P. Schönheit, unpublished) and probably other hyperthermophilic archaea. The apparent absence of allostery is not simply a consequence of thermostability, as PK from *Thermotoga maritima*, a hyperthermophilic bacterium that thrives at temperatures up to 90 °C, exhibits conventional regulatory properties.[16] *Pa*PK is also unusual in that it binds ADP cooperatively and shows no response to AMP.[16] Why PK should exhibit cooperative but not allosteric regulation is perplexing and appears to be at odds with its importance as a major regulatory step of glycolysis. A further distinguishing feature of *Pa*PK is that it is a member of a small subset of PK enzymes that does not require a monovalent cation (NH_4^+ or K^+) for activity.[16]

To understand its unusual properties and to shed light on how this enzyme functions in the modified glycolysis of a hyperthermophilic crenarchaeon, we determined the crystal structure of *Pa*PK at 2.2 Å resolution, the first structure of a PK from an archaeon and from a hyperthermophile. Surprisingly, the structure reveals a bound sulfate or phosphate in the C domain at a position corresponding to the 5′- or 6′-phosphate of allosteric effectors, suggesting that, contrary to expectations, an allosteric site is present in the enzyme. The region that would otherwise accommodate the furanose rings of R5P or FBP appears to be blocked by a tyrosine, but an adjacent cavity that could bind smaller intermediates is apparent. A search of phosphorylated three-carbon intermediates of glycolysis revealed 3-phosphoglycerate as a potent allosteric activator of *Pa*PK. Regulation of *Pa*PK by a carboxylic acid contrasts sharply with other PKs, which are all activated by sugar phosphates. Thus, *Pa*PK may represent an early stage in the evolution of glycolysis when regulation was mediated by noncarbohydrate intermediates from the lower half of the pathway.

EXPERIMENTAL PROCEDURES

Protein Expression and Purification. The cloning, expression, and purification of *Pa*PK have been reported previously;[16] the full-length protein (without any His tag) was expressed using a pET17b vector, but a slightly modified procedure for purification was used here. Four liters of *Escherichia coli* BL21 DE3 pLysS Codonplus cells (Stratagene Inc.) that had been transformed with the pET17b vector were grown to an OD_{600} of ∼0.6 at 37 °C. Expression of *Pa*PK was then induced by addition of 0.5 mM IPTG, and the cells were grown for a further 4 h. After being harvested by centrifugation (2000*g* for 30 min) and resuspended in 50 mM NaCl and 50 mM Tris-HCl (pH 7.5), the cells were lysed by sonication, and the cell debris was pelleted by high-speed centrifugation (25000*g* for 25 min). To precipitate *Pa*PK, 0.4 g/mL solid ammonium sulfate was added to the cell lysate, and then the mixture was stirred on ice for 1 h. Following centrifugation (25000*g* for 25 min), the resulting pellet was resuspended in 50 mM Tris (pH 7.5) and 50 mM NaCl, and nonthermostable proteins were removed when the sample was heated at 80 °C for 30 min, followed by centrifugation. The supernatant was then dialyzed overnight against 50 mM Tris-malonate buffer (pH 5.3) and applied to a HiTrap SP ion exchange column (GE Healthcare) (equilibrated in the same buffer), and the protein was eluted with a linear gradient from 0 to 1 M NaCl. Fractions containing *Pa*PK were pooled and concentrated to ∼5 mL, followed by buffer exchange into 20 mM Tris (pH 7.5) and 50 mM NaCl using a Centricon-30 concentrator (Millipore, Inc.). Finally, the protein was passed across a Superose 400-GL gel filtration column (GE Healthcare) (equilibrated in the same buffer), and a single peak eluted at ∼200 kDa (the expected mass of a *Pa*PK tetramer). The protein was >95% pure, as judged by sodium dodecyl sulfate−polyacrylamide gel electrophoresis.

Pyruvate kinase (pykF) from *E. coli* (type I), which is allosterically regulated by FBP, was expressed in *E. coli* strain pCA24N*pykF* JW1666 (obtained from U. Sauer, ETH, Zürich, Switzerland), and the His-tagged enzyme was purified by standard procedures. Activity was measured at 25 °C as described previously,[27] except that the buffer consisted of 40 mM HEPES (pH 7.4), 10 mM $MgCl_2$, 50 mM KCl, and 0.2 mM PEP.

Site-Directed Mutagenesis and Activity Measurement. Mutants of *Pa*PK were generated using the QuikChange protocol (Stratagene, Inc.) and then purified in the same way as the wild-type enzyme. Activity measurements followed previously described procedures.[16] Briefly, the enzyme was assayed at 65 °C in 100 mM BisTris (buffered at pH 6.2) containing 1−10 mM PEP, 2 mM ADP, 5 mM $MgCl_2$, 0.3 mM NADH, and one enzyme unit of rabbit muscle LDH. The response of *Pa*PK to potential effectors, each at a concentration of 1 mM, was measured at 1 mM PEP.

Crystallization. *Pa*PK was concentrated to 5.5 mg/mL and subjected to crystallization trials by the hanging-drop vapor-diffusion method. Initially, the protein was screened against Crystal Screens I and II (Hampton Research Inc., Palo Alto, CA) in which a drop containing 2 μL of protein solution was mixed with 2 μL of well solution and suspended over 1 mL of well solution. Small, needle-like crystals appeared after incubation for 1 week at 18 °C over a well containing 8% PEG 8000 and 0.1 M Tris-HCl (pH 8.5). After optimization, the largest crystals were obtained after 1 week over wells containing 17% PEG 1500 and 100 mM Tris-HCl (pH 8.2). These were clusters of plates with approximate dimensions of 0.4 mm × 0.4 mm × 0.02 mm. Diffraction analysis indicated the crystals belong to space group *C*2 with two molecules in the asymmetric unit and the following cell dimensions: a = 116.3 Å, b = 107.4 Å, c = 105.0 Å, and β = 110.6°.

X-ray Data Collection and Structure Determination. Crystals were cryoprotected by being passed through a series of mother liquor solutions [17% PEG 1500 and 100 mM Tris-HCl (pH 8.2)] containing increasing amounts of glycerol (in 2% increments) to a final concentration of 28% glycerol (v/v) and then flash-frozen *in situ* in a cryostream (X-stream 2000, Rigaku-MSC); 270° of data was collected at a wavelength of 1.00 Å on a MAR-225 CCD detector at the SER-CAT BM-22 beamline at the Advanced Photon Source (APS), Argonne National Laboratory (Argonne, IL). The data were collected in 1° increments with an exposure time of 5 s per frame, and the crystal-to-plate distance was 250 mm. Data were processed and scaled with HKL2000[28] to 2.2 Å resolution and reduced with an R_{merge} of 5.3% and 99% completeness (see Table 1). The structure was determined by molecular replacement using MOLREP[29] with subunit A of the structure of PK from *Leishmania mexicana* (*Lm*PK) as a search model.[30] *Lm*PK exhibits 22% amino acid sequence identity with *Pa*PK. The model was refined with iterative rounds of model building and

Table 1. X-ray Diffraction Data and Model Refinement Statistics for the Crystal Structure of *Pa*PK

Data Collection[a]	
space group	C2
cell dimensions	
a, *b*, *c* (Å)	116.3, 107.4, 105.0
α, *β*, *γ* (deg)	90.0, 110.7, 90.0
resolution range (Å)	39.0−2.20 (2.28−2.20)
R_{merge} (%)	5.3 (40.3)
completeness (%)	99.7 (98.3)
redundancy	3.6 (3.3)
$\langle I\rangle/\langle\sigma I\rangle$	33.3 (3.5)
no. of unique reflections	60944 (5983)
Refinement	
resolution (Å)	39.0−2.2
no. of non-hydrogen protein atoms	6887
no. of water molecules	140
R_{cryst}/R_{free} (%)	20.7/24.7
rmsd from ideal stereochemistry	
bond lengths (Å)	0.012
bond angles (deg)	1.37
B factor	
mean *B* factor (main chain) (Å^2)	47.6
rmsd in main chain *B* factors (Å^2)	0.70
mean *B* factor (side chains and waters) (Å^2)	48.6
rmsd in side chain *B* factors (Å^2)	1.59
Ramachandran plot (%)	
residues in most favored regions	91.9
residues in disallowed regions	7.6
residues in generously allowed regions	0.3
residues in disallowed regions	0.3
PDB entry	3QTG

[a]Numbers in parentheses are for the outer resolution shells.

automated refinement, using O[31] and REFMAC,[32] respectively. The final model includes three sulfates, and alternate conformations were modeled for five residues. As determined using PROCHECK,[33] 91.9% of residues lie in the most favored region of the Ramachandran plot, with 7.6% in additionally allowed regions, 0.3% in generously allowed regions, and 0.3% in a disallowed region. The electron density for all Ramachandran outliers is excellent. Additional density next to the side chain of Ser157 (of molecule A in the asymmetric unit) suggests that this residue may be modified in some way during protein expression, perhaps by phosphorylation. The same residue in molecule B is not visible because of disorder in the B domain.

RESULTS

Structural Description. The structure of *Pa*PK was determined at 2.2 Å resolution (Figure 1 and Table 1) from a crystal in which the asymmetric unit comprises two subunits of the homotetramer. As with PKs with known structure,[13,30,34−39] each subunit of the enzyme consists of three domains. The A domain is an 8*α*-8*β* TIM barrel and contains the active site. The B domain is linked to the A domain by a flexible hinge region and is predominantly of *β* structure. In both rabbit PK and *Lm*PK, this domain closes down upon the active site upon binding of ADP.[14,40] The C domain consists of an *α*−*β*−*α* sandwich and in allosteric PKs contains the binding site for the allosteric effector.[13] Within the tetramer, there are two intersubunit interfaces: the A−A interface between adjacent A domains and the C−C interface between adjacent C domains.

Most of the crystal structure of *PaPK* has well-defined electron density, but some areas were not modeled because of weak or absent electron density. These include the first 11 residues of molecule A and 14 residues of molecule B, as well as residues 88−95, 107−116, and 156−165 (inclusive) of the B domain in molecule B of the asymmetric unit. The apparent disorder of the B domain of molecule B may be due to the lack of crystal contacts involving this domain compared to the same domain in molecule A. In addition, the B domain of molecule B lies slightly farther from the A domain than in molecule A

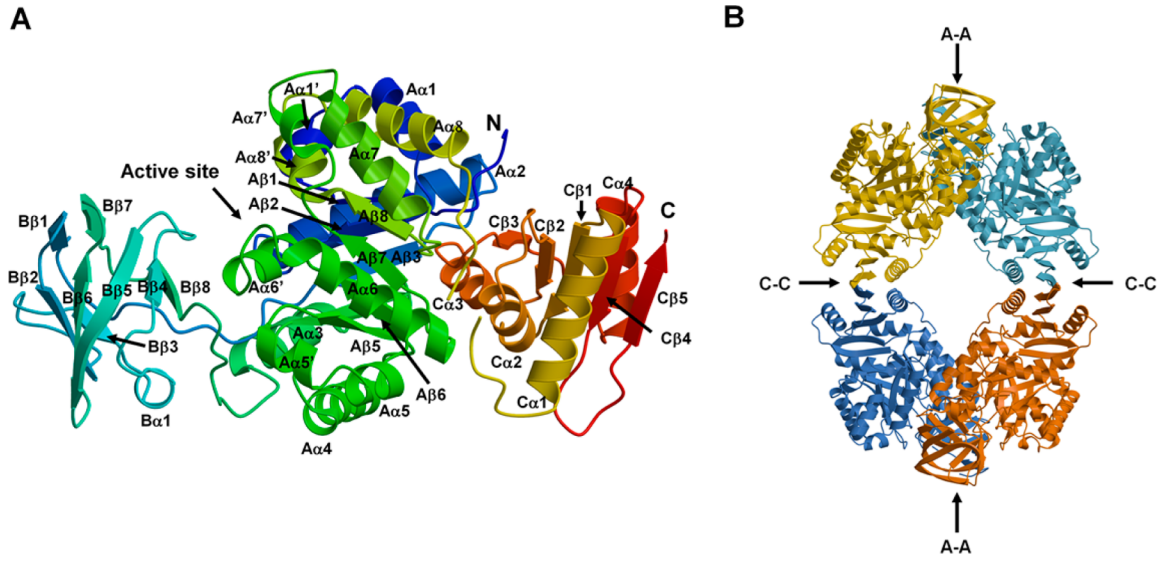

Figure 1. Crystal structure of pyruvate kinase from *Pyrobaculum aerophilum* (*Pa*PK). (A) Single subunit of *Pa*PK (molecule A) showing the domain structure of the enzyme. The molecule is displayed in ribbon format and color-ramped blue (N-terminus) to red (C-terminus). The elements of secondary structure are labeled. (B) Tetramer of *Pa*PK constructed by applying crystallographic symmetry to the asymmetric unit and showing the two interfaces. Secondary structure assignments are shown in Figure S1 of the Supporting Information.

dx.doi.org/10.1021/bi400761b | *Biochemistry* 2013, 52, 5865−5875

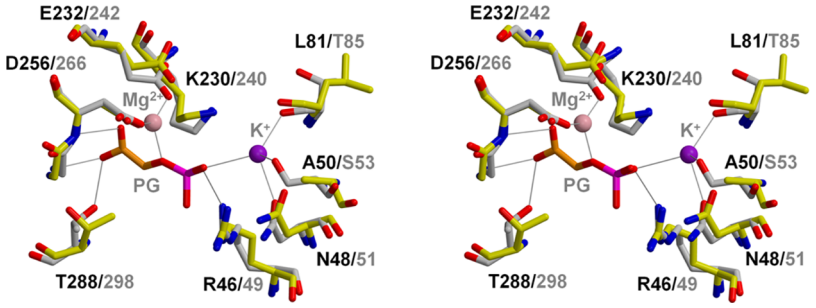

Figure 2. Superimposition of the active sites of *Pa*PK (yellow) and yeast pyruvate kinase (*Sc*PK) (gray) showing the sequence conservation between the two enzymes. Residues are labeled in black for *Pa*PK and gray for *Sc*PK. The structure of *Sc*PK used for the superimposition is the complex with phosphoglycolate (PG), Mg^{2+}, and K^+.[13] Potential hydrogen bonds are shown as thin lines.

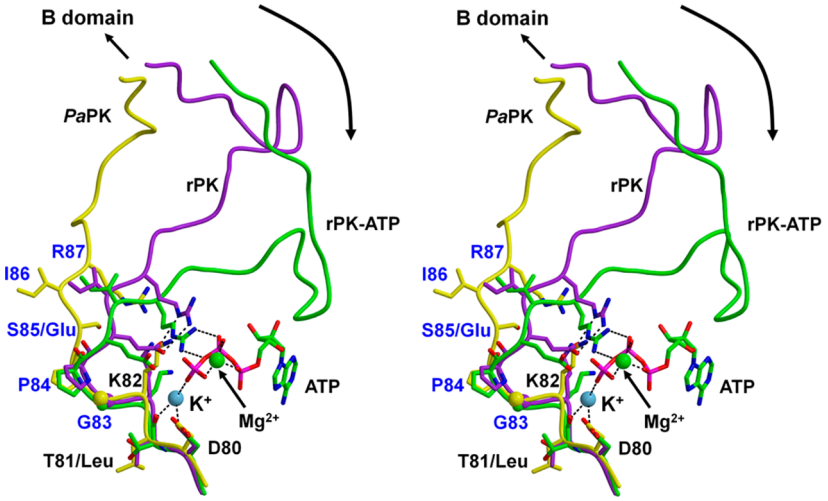

Figure 3. Nucleotide-binding region of *Pa*PK and conserved GPXIR motif. This stereoview shows a superimposition of the backbone of *Pa*PK (yellow) with structures of rabbit PK (rPK) determined in the absence (purple) and presence (green) of ATP.[36,40] ATP from the complex of rabbit PK is colored with green bonds; K^+ (present in both rabbit PK structures) is shown as a blue sphere, and Mg^{2+} is shown as a green sphere. Note the relative positions of the connecting loop from the A domain to the B domain that contains the GPXIR motif, labeled in blue, showing how residues of this loop shift toward the active site upon binding the nucleotide. Potential hydrogen bonds are shown as dashed lines.

(Figure S2 of the Supporting Information). This aside, the respective A and C domains overlap closely in the two molecules, with a root-mean-square deviation between common main chain atoms of 0.26 Å.

The active site of PK lies at the top of the TIM barrel in a cleft between the A and B domains (see Figure 1A). The electron density for all residues in the active site is well resolved except for that of Asp256, whose side chain is not fully visible in the $|F_o| - |F_c|$ difference electron density (Figure S3 of the Supporting Information). This residue coordinates Mg^{2+}, and the absence of such an ion in the crystal structure may explain the weak density for this side chain. When compared with those of yeast PK (*Sc*PK), as a representative of the PK family, the majority of residues in the active site of *Pa*PK are conserved (Figure 2).

Basis for the K^+ Independence of *Pa*PK. Many PKs require a monovalent cation for activity (K^+ or NH_4^+), and it is believed to assist in formation of the active conformation of the enzyme.[41] The structure of *Pa*PK is the first of a PK that does not require K^+ for activity. The comparison with *Sc*PK, which is potassium-dependent, shows two differences in the potassium-binding region (Figure 2). One of these, a leucine at position 81 of *Pa*PK in place of a threonine observed in other PKs, is a conservative one because the carbonyl of Leu81 coordinates K^+ in the same way as the Thr carbonyl of other PKs. An alanine at position 50 in place of a serine observed in K^+-dependent PKs is a more significant difference, as this removes a hydroxyl that coordinates with K^+. This difference alone, though, may not explain the potassium independence of *Pa*PK. Type II PK of *E. coli* contains a serine at this position yet is also potassium-independent[42] (for an alignment of PK sequences, see Figure S1 of the Supporting Information).

Another region linked with K^+ dependence in PK is the GPXIR motif (where the X is variable) that lies on the boundary between the A and B domains near the potassium-binding site. In K^+-dependent PKs, X is a glutamate that may balance the charge of K^+,[40] and in K^+-independent PKs, it is a lysine that may mimic the positive charge of K^+.[42,43] In rabbit PK (K^+-dependent), the residues of this motif act as a hinge during closure of the B domain onto the active site after binding ADP[40] (Figure 3), and a similar transition is also seen in *Lm*PK.[14] *Pa*PK belongs to a very small and unique cluster of K^+-independent PKs, all from archaeal organisms, in which the X is a serine residue.[43] Upon similar closure of the B domain, Ser85 most likely forms a hydrogen bond with Arg87, which interacts with the β-phosphate and Mg^{2+} and thus may help to position ADP optimally for phosphoryl transfer (Figure 3). Why a serine correlates with the K^+ independence of *Pa*PK, however, remains unclear because it appears to be too distant

dx.doi.org/10.1021/bi400761b | *Biochemistry* 2013, 52, 5865−5875

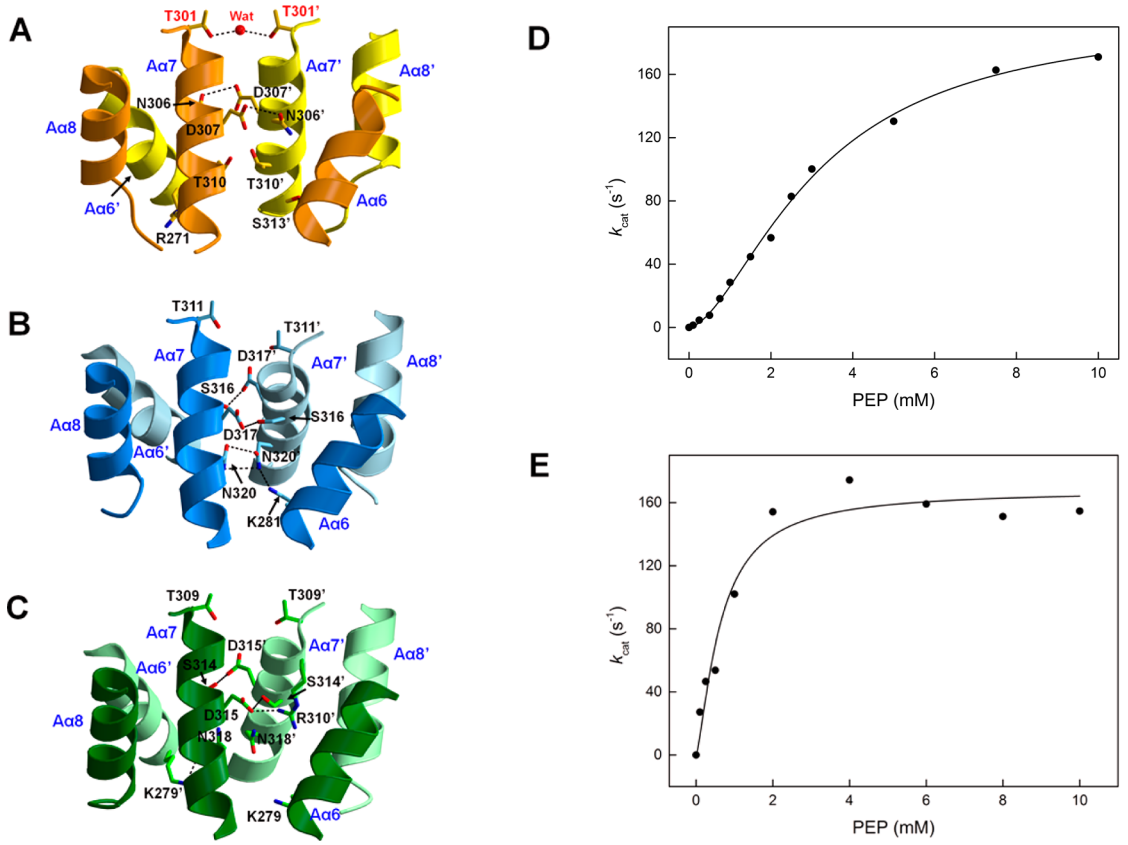

Figure 4. A–A interface of pyruvate kinase and its role in cooperativity. Shown are the respective A–A interfaces of (A) *Pa*PK, (B) *Sc*PK, and (C) *L. mexicana* PK (*Lm*PK) in which subunits are distinguished by light or dark coloring. In each case, side chains involved in interactions are shown and dashed lines represent potential hydrogen bonds (a prime denotes the adjacent subunit at the interface). The structure used for *Sc*PK is the complex with FBP,[13] and the structure for *Lm*PK is that with sulfate bound at the 1′-phosphate of the allosteric effector.[52] For *Pa*PK, the position of Thr301, which bridges with its counterpart across the interface via a water molecule, is labeled in red. The role of Thr301 in the cooperative response of *Pa*PK was tested by its mutation to Val to eliminate the hydrogen bond with the water molecule. (D) Cooperative binding kinetics of PEP with wild-type *Pa*PK, showing a sigmoidal curve. (E) The Thr301Val mutant shows Michaelis–Menten kinetics, commensurate with a loss of cooperativity.

from the site of phosphoryl transfer, even after a shift of domain B toward the active site.

Structural Comparison with Other PKs. Superimposition of the structure of *Pa*PK with those of other PKs, including those of *E. coli* type I,[37] yeast,[13] and *L. mexicana*,[30] shows a close overlap of individual subunits irrespective of whether the structure contains a bound effector molecule (Figure S4 of the Supporting Information). The closest correspondence occurs in the A domain, with more divergence apparent in the C domain (see below). The relative position of the B domain varies in different PK structures when the enzyme is crystallized in the apo state, and the superimpositions indicate that *Pa*PK exists in an open state with respect to the B domain. To determine whether the structure of *Pa*PK represents the T or R state, a tetramer was constructed by applying crystallographic symmetry to the A–A "dimer" of the asymmetric unit (see Figure 1A) and superimposed onto the structure of apo *Lm*PK (PDB entry 1PKL), which is in the T state.[30] All subunits overlap closely, indicative of the *Pa*PK structure being in the T state (Figure S5 of the Supporting Information). Superimposition of the *Pa*PK A–A dimer with an A–A dimer extracted from the tetrameric crystal structure of *Lm*PK in the R state (PDB entry 3HQP) shows a relative shift of domains. This corresponds to the allosteric transition that has been documented in a series of *Lm*PK structures, involving rigid body motions of the AC domain cores.[14]

Regulatory Pathway in the A Domain of *Pa*PK. Given that *Pa*PK is tetrameric in solution,[16] it is presumed that both the A–A and C–C interfaces are involved in the transmission of regulatory signals between active sites in the tetramer (see Figure 1B). A network of noncovalent interactions involving conserved side chains that links the active and allosteric sites with both interfaces has been proposed as a pathway for the transmission of regulatory signals in *Sc*PK.[44] Much of this pathway is present in the A domain of *Pa*PK, suggesting a conservation of signaling mechanisms within this domain of PK. In fact, both the arrangement of helices at the A–A interface and the residues that mediate interactions are conserved in different PK enzymes (Figure 4A–C). To confirm the involvement of the A–A interface in regulation in *Pa*PK, we mutated Thr301 to valine. This residue is located at the N-terminal cap position of Aα7, which is the key helix at the A–A interface and corresponds to the same position as a Thr to Met mutation in human PK that lowers the responsiveness of mammalian PK to FBP. It is also associated with the Tokyo/Nagasaki/Beirut form of hemolytic anemia.[45,46] In the crystal structure of *Pa*PK, the threonine hydroxyl interacts with its counterpart in the neighboring molecule across the A–A interface via a bridging water molecule. By mutating to valine, the goal was to remove this hydrogen bonding interaction across the interface. The T301V mutant was purified, and size-exclusion chromatography showed the mutant had not altered

dx.doi.org/10.1021/bi400761b | *Biochemistry* 2013, 52, 5865–5875

the tetrameric state of *Pa*PK. The T301V mutation abolished the cooperative response of *Pa*PK with an unchanged V_{max} (Figure 4D,E), suggesting that it may have a role in regulatory signaling or that it is a critical residue for the architecture of Aα7 at the A−A interface. The T311M mutation in *Sc*PK similarly causes loss of cooperative behavior but also reduces enzyme activity.[44]

C−C Interface. When compared with those of other PKs, the C domain of *Pa*PK is structurally less conserved than the A domain. For instance, the first segment of this domain (residues 345−355), which follows the A domain, is comprised of an irregular loop in *Pa*PK, whereas the equivalent region in *Sc*PK[13] and *Lm*PK[30] is longer and helical (called Cα1) (Figure 5). In *Pa*PK, the C−C interface is comprised of interactions between Cα1 and Cβ5, with the latter forming a β sheet with its counterpart across the interface. Of significance for the transmission of regulatory signals, the residues comprising the interface helix (Cα1 in *Pa*PK) are very different compared those of the equivalent helix in *Sc*PK and *Lm*PK (called Cα2).

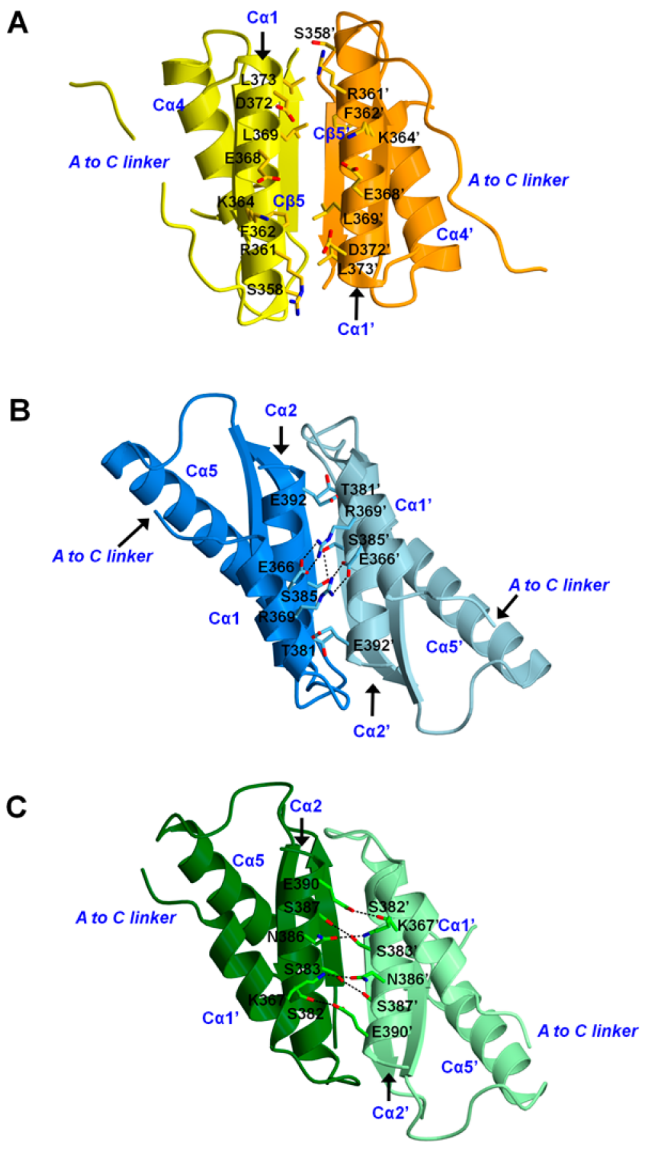

Figure 5. Structure of the C−C interface in (A) *Pa*PK, (B) *Sc*PK, and (C) *L. mexicana* PK (*Lm*PK), using the same structures and representation as in Figure 4.

Whereas there are numerous hydrogen bonding or electrostatic interactions between side chains of Cα2 in *Sc*PK and *Lm*PK, there is dearth of such interactions in Cα1 of *Pa*PK, with Asp372 and Arg361 being the only two charged side chains that could potentially interact. A distinctive feature of the interface is a line of hydrophobic residues (Phe362, Leu366, Leu369, and Leu373) along Cα1 that packs into the hydrophobic core of the interface space. Such features may dictate the respective allosteric properties of *Pa*PK compared to those of conventional PKs.

A Putative Allosteric Site in the C Domain of *Pa*PK. Unexpectedly, electron density consistent with a bound sulfate or phosphate ion was observed in the C domain in both molecules of the asymmetric unit of *Pa*PK (Figure 6A). Initially, these peaks were interpreted as a sulfate because ammonium sulfate was used during purification of the protein, but since they were also observed in crystal structures determined from protein purified in the absence of sulfate (data not shown), they could be due to a copurified phosphate. Each sulfate (or phosphate) ion is within hydrogen bonding distance of three main chain amides (Met382, Ser383, and Thr385) and the side chain hydroxyl group of Ser381, which are all present on the Cβ1−Cα2 loop. An additional contact is made by the hydroxyl group of Tyr428, which emanates from Cα4. Superimposition of the structure of *Pa*PK with that of *Sc*PK in complex with FBP[13] reveals that the sulfate overlaps almost exactly with the 6′-phosphate of FBP bound in the effector-binding pocket (Figure 6B) and is very suggestive that *Pa*PK does in fact contain an allosteric site. The same is also true upon superimposition onto the structure of *Lm*PK in complex with F-2,6-BP[14] (Figure S6 of the Supporting Information). The superimposition also indicates why *Pa*PK does not respond to either R5P or FBP[16] because the space that would be occupied by the furanose rings of a sugar phosphate effector is occluded by Tyr428. The reason behind this occlusion is the proximity of Cα4, relative to its counterpart in *Sc*PK (Cα5), which brings the tyrosine closer to the sulfate or phosphate position, whereas the equivalent residue in *Sc*PK (Trp452) is much more distant.

3-Phosphoglycerate (3PG) Is an Allosteric Activator of *Pa*PK. Although the region of the putative allosteric site that would otherwise bind the furanose ring of FBP appears to be occluded by Tyr428, examination of the structure revealed a cavity between Cα1 and Cα2 that could be a binding site for a different phosphorylated intermediate. *Pa*PK does not respond to any phosphorylated intermediate of the upper half of glycolysis,[16] and because the lower half of the glycolytic pathway uses only three-carbon intermediates, the enzyme activity of *Pa*PK was measured in the presence of these, as well as phosphate. Dihydroxyacetone phosphate (DHAP), glyceraldehyde 3-phosphate (GAP), 2-phosphoglycerate (2PG), and phosphate did not stimulate *Pa*PK and acted as weak inhibitors (Table S1 of the Supporting Information). Interestingly, their inhibitory effect was weakened in an S381A/Y428A mutant, in which two of the residues that contact the sulfate were mutated to alanine, suggesting these bind to the phosphate-binding site in the C domain and act as weak negative regulators. By contrast, addition of 1 mM 3-phosphoglycerate (3PG) led to potent activation of the enzyme and altered the kinetics of PEP from a sigmoidal response to hyperbolic, consistent with allosteric activation of the enzyme (Figure 7A). At 1 mM PEP, maximal activity was observed at ∼0.5 mM 3PG, corresponding to a 5-fold stimulation, from 24.9 to 124.5 s^{-1} (Figure 7B), and

dx.doi.org/10.1021/bi400761b | *Biochemistry* 2013, 52, 5865−5875

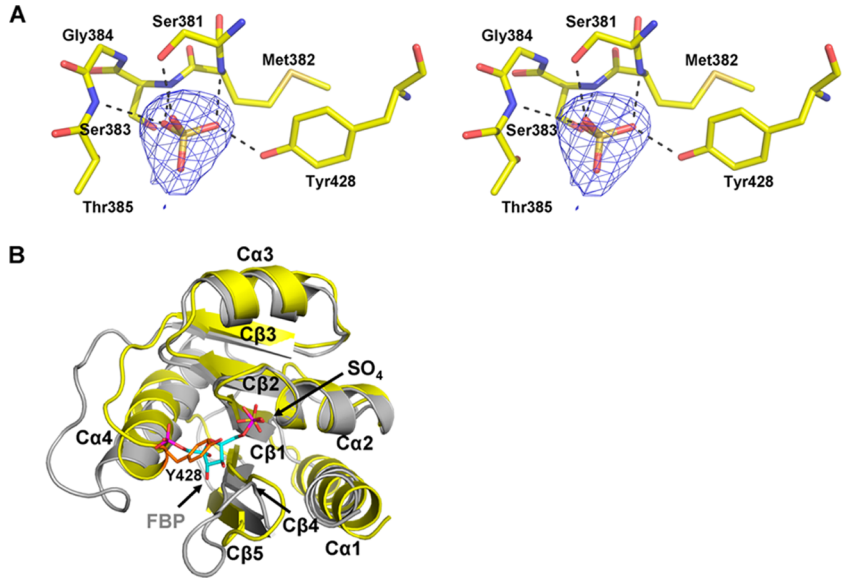

Figure 6. Molecule of sulfate (or phosphate) bound in the C domain of *Pa*PK. (A) Stereoview showing the $|F_o| - |F_c|$ difference electron density corresponding to the sulfate, contoured at 3.5σ, bound by residues in the loop preceding Cα2. (B) Superimposition of *Pa*PK (yellow) with *Sc*PK (gray) in complex with fructose 1,6-bisphosphate (FBP) (blue bonds)[13] showing the overlap of the sulfate (orange bonds) with the 6′ position of the allosteric effector. Note the overlap of Tyr428 of *Pa*PK with the furanose ring of FBP. Secondary structure elements of *Pa*PK are labeled.

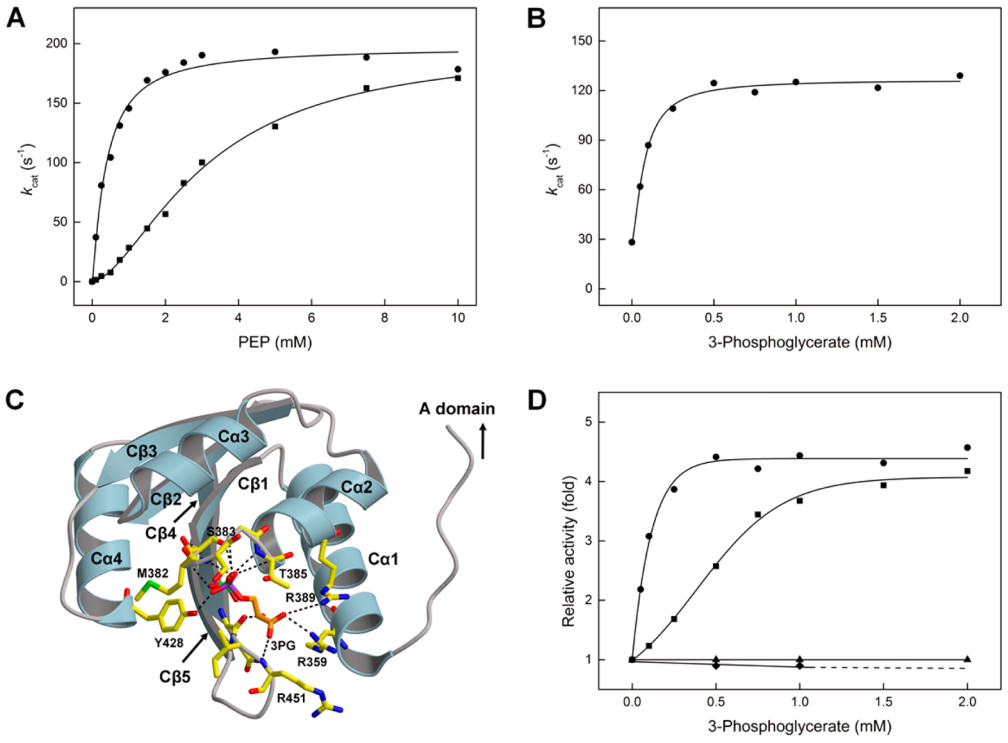

Figure 7. 3-Phosphoglycerate (3PG) is a potent allosteric activator of *Pa*PK. (A) Plot of the specific activity of *Pa*PK vs increasing concentrations of PEP in the presence (●) and absence (■) of 1 mM 3-phosphoglycerate. 3PG resulted in a change in the sigmoidal kinetics (Hill coefficient of 1.9) to hyperbolic Michaelis−Menten kinetics (apparent K_m of 0.48 mM). (B) Stimulation of *Pa*PK as a function of 3PG concentration at 1 mM PEP. (C) 3PG modeled into a cavity of the C domain that lies between Cα1 and Cα2 of the C domain. The backbone of the C domain is shown as a blue ribbon, and residues that surround 3PG are displayed as yellow bonds. 3PG is colored with orange bonds, and the bound sulfate (that was used to guide the docking) is also shown with green bonds. (D) Effect of 3PG on relative *Pa*PK activities of the wild type, R359A, R389A, and Y428A/S381A. The activities were measured at 1 mM PEP, 2 mM ADP, and 5 mM $MgCl_2$. For the S381A/Y428A double mutant, the dashed line reflects the fact that 3PG was tested up to 5 mM. The relative activity of 1 indicates PK activity in the absence of 3PG and corresponds to 28.2 s^{-1} for the wild type (●), 16.2 s^{-1} for R359A (■), 21.6 s^{-1} for R389A (▲), and 34.4 s^{-1} for Y428A/S381A enzymes (◆).

at 0.25 mM PEP, the stimulation was even stronger (18-fold, from 4.56 to 80.5 s^{-1}). A 12-fold stimulation (from 5 to 60 milliunits/mg at 0.2 mM PEP) was also observed in the presence of 2 mM 3PG when PK activity was measured in cell extracts of *P. aerophilum*, showing that activation also occurs *in vivo* and is not an artifact of protein purification. Significantly

dx.doi.org/10.1021/bi400761b | *Biochemistry* 2013, 52, 5865−5875

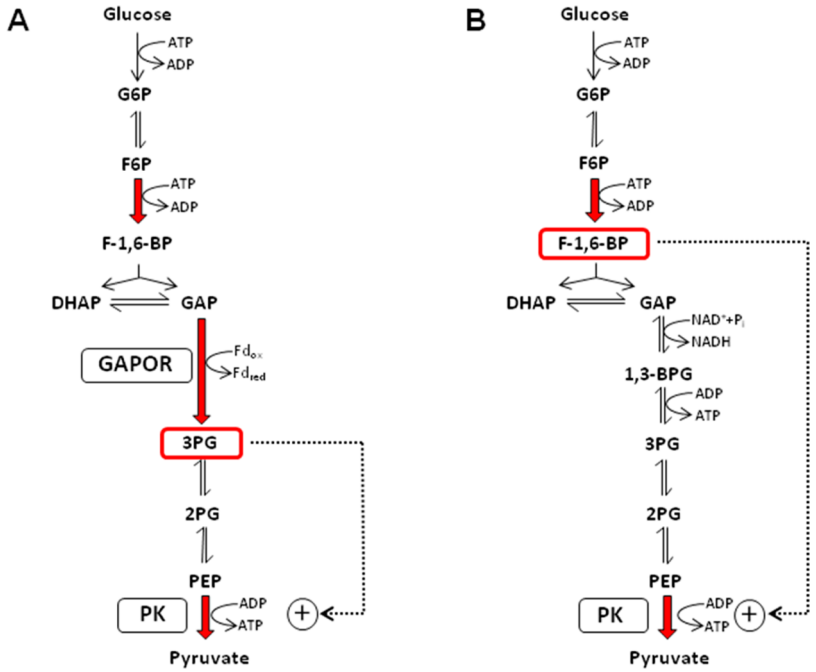

Figure 8. Classical Embden–Meyerhof (EM) pathway and its modification in the hyperthermophilic archaeon *P. aerophilum*. This schematic shows (A) the modified EM pathway of *P. aerophilum* and (B) the classical EM pathway of eukarya and bacteria. Irreversible enzymes that operate in each pathway are designated by red arrows, and intermediates that activate PK are shown in red boxes.

less stimulation (3.5-fold, from 2.6 to 9.3 s^{-1} at 0.25 mM PEP) was observed using protein purified with an ammonium sulfate step than using protein purified in its absence. This suggests that occupation of the phosphate-binding site by sulfate can conceal the allosteric effect. Importantly, no stimulation of the S381A/Y428A double mutant was observed with 1 mM 3PG at PEP concentrations between 0.25 and 1 mM, confirming that 3PG binds to the phosphate-binding site in the C domain.

To determine whether an FBP-activated PK could also respond to 3PG, *E. coli* pykF was purified and tested for stimulation by FBP and 3PG. In the presence of 0.2 mM PEP, addition of 2 mM FBP resulted in a 40-fold increase in the activity of pykF (from 0.24 to 9.77 s^{-1}). By contrast, at the same PEP concentration, addition of 2 mM 3PG did not increase the activity of pykF. Hence, it appears that FBP-activated PKs are not regulated by 3PG.

To understand how 3PG might bind in the C domain of *Pa*PK, the molecule was manually docked into the crystal structure of the enzyme, using the bound sulfate as an initial guide. With Tyr428 blocking what would be the canonical allosteric binding site of PK, the molecule was positioned within a cavity on the opposite side, between helices Cα1 and Cα2, and a β hairpin comprising Cβ4 and Cβ5 at the C terminus of the protein (Figure 7C). This docking brings the carboxylate group of 3PG close to the side chains of two arginines (359 and 389), and one of these presumably counteracts its negative charge. The carboxylate also contacts the main chain amide of Arg451. Interestingly, one of the arginines (Arg359) lies at the N-terminal end of Cα1, whose preceding loop connects directly from the A domain.

To test this model, the two arginines whose side chains were proposed to contact 3PG were mutated and the effect on the allosteric response was measured (Figure 7D). As in the S381A/Y428A mutant, mutation of Arg389 to Ala abolished the stimulation. For the R359A mutant, maximal stimulation required a 3-fold higher concentration of 3PG (~1.5 mM), compared to that of wild-type *Pa*PK (~0.5 mM). Hence, mutation of residues proposed to contact both the phosphate and the carboxylate regions of 3PG abolished or diminished the allosteric response. Overall, these data identify 3PG as a novel and potent allosteric activator of *Pa*PK and suggest that the effector binds in the C domain of the protein, with only the phosphate-binding site being shared with the canonical allosteric site for PK.

DISCUSSION

We selected pyruvate kinase from *P. aerophilum* for structural studies because it exhibits cooperativity for its substrate but is apparently nonallosteric because it does not respond to any known effector of PK. Our discovery that 3-phosphoglycerate (3PG) is a potent allosteric effector, however, immediately challenges this view. As indicated by the lack of a similar response with GAP (the corresponding aldehyde) or 2PG (where the phosphate is in the 2 position), the allosteric response of *Pa*PK is highly specific for 3PG.

The proposed binding site for 3PG in the C domain of *Pa*PK was confirmed by mutation of residues proposed to contact the carboxylate and phosphate groups of 3PG. Because the region occupied by the furanose ring in the canonical allosteric site of PKs is blocked by Tyr428 in *Pa*PK, only the phosphate-binding motif formed by the connecting loop between Cα2 and Cβ2 is conserved. This means that the one consistent feature of all known allosteric effectors of PK (FBP, R5P, AMP, F-2,6-BP, and now 3PG) is the phosphate, which suggests its recognition is of primary importance for the allosteric mechanism of PK. The specificity of allosteric effectors with respect to the transmission of regulatory signals at the C–C interface is therefore most likely governed by interaction with the furanose or pyranose ring of sugar phosphates and in *Pa*PK by interaction with the 2-hydroxyl and carboxylate of 3PG. In the case of *Pa*PK, mutation of a single arginine proposed to

dx.doi.org/10.1021/bi400761b | *Biochemistry* 2013, 52, 5865–5875

interact with the carboxylate of 3PG (Arg389) is sufficient to abolish the response.

This is not the first instance of a sulfate binding in the C domain in an apparently nonallosteric PK, because a very similar situation has been observed very recently with PK from *Cryptosporidium parvum*, a protozoan parasite (*Cp*PK).[47] Like *Pa*PK, *Cp*PK does not respond to any known effector molecules,[48] yet a sulfate derived from the crystallization solution was observed in the crystal structure bound at a position equivalent to the 6′-phosphate of known effectors of PK. In sharp contrast to *Pa*PK, however, the region that would accommodate the ring of a sugar phosphate effector is open, so it is most likely that *Cp*PK is in fact allosterically regulated by a sugar phosphate, but one of unknown identity. As we have performed for *Pa*PK, a wider search for potential effectors of *Cp*PK appears to be necessary.

The nature of the allosteric transition in *Pa*PK is likely to be very similar to that revealed by the extensive structural analysis of *Lm*PK. This indicates a 6° rotation of the AC domain core around a pivot point at the base of the TIM barrel that alters the quaternary structure of the enzyme.[14] Superimposition of the asymmetric unit of *Pa*PK, comprising an A−A "dimer", with *Lm*PK in the R state shows how a very similar rotation could also occur in *Pa*PK (Figure S5 of the Supporting Information). In the so-called "roll and lock" mechanism of *Lm*PK, the R state is stabilized by four new electrostatic interactions formed at the C−C interface as a result of binding F-2,6-BP. Arg361 and Asp372 are present at the C−C interface of *Pa*PK and in the current structure do not interact with each other across the interface but might move to do so upon binding of 3PG.

The discovery that 3PG is a potent activator of *Pa*PK has implications for our understanding of how glycolysis is regulated in *P. aerophilum*. In the unmodified, classical EM pathway, the activation of eukaryotic and type I prokaryotic PKs by FBP, the product of the irreversible enzyme phosphofructokinase (PFK), is a mechanism for coordinated regulation between the upper and lower sections of glycolysis to ensure that both act in concert (Figure 8). Consistent with this, the activity of *E. coli* type I PK (pykF), tested as an example of a classically regulated PK, increased by 40-fold upon addition of FBP but did not respond to 3PG. The situation is quite different in the modified EM pathway of *P. aerophilum* because, although FBP is also produced irreversibly,[25] it does not activate *Pa*PK. Instead, *Pa*PK responds to 3PG, which is formed in the lower half of the glycolytic pathway. One reason for this strikingly different metabolic arrangement may lie in the reaction that produces 3PG. In *P. aerophilum*, 3PG is generated by glyceraldehyde 3-phosphate ferredoxin oxidoreductase (GAPOR)[25] via an irreversible oxidation of glyceraldehyde 3-phosphate (GAP) to 3PG, a reaction that is unique to EM pathways of phylogenetically ancestral archaea. By contrast, in the classical EM pathway, the oxidation of GAP to 3PG is catalyzed by two reversible enzymes, glyceraldehyde-3-phosphate dehydrogenase (GAPDH) and phosphoglycerate kinase (PGK). Hence, coordinated regulation of PK does appear to occur in *P. aerophilum* but involves interaction with an irreversible step in the lower half of the pathway. It has been argued that the marked diversity of enzymes in the EM pathway of heterotrophic archaea is the result of convergent adaptation as a response to the growing abundance of sugar substrates derived from cyanobacterial and plant cell walls.[49] If so, then regulation of *Pa*PK by a noncarbohydrate allosteric effector may be a remnant of a stage in evolution that predates sugar metabolism.

A remaining question is whether regulation of PK by 3PG also occurs in other archaeal species. Although a wider survey is needed, early indications are that such regulation is specific for *P. aerophilum* because although PKs from *Thermoproteus tenax* and *A. pernix* are 32 and 47% identical with *Pa*PK, respectively, neither responds to 3PG[26](U. Johnsen and P. Schönheit, data not shown). Homology modeling of these enzymes shows that *A. pernix* PK lacks an equivalent to Arg359 and Arg451 and, although *T. tenax* PK has equivalents for both, it lacks the two β strands at the C-terminal end of *Pa*PK, and thus, the binding site appears to be incomplete (data not shown). Hence, PK in these species may be regulated by other mechanisms, and in *T. tenax*, PK is regulated at the transcriptional level.[26]

To conclude, we have discovered that 3PG is an allosteric effector of *Pa*PK. Metabolic regulation by a small carboxylic acid as opposed to the sugar phosphates of conventional effectors of pyruvate kinase is unexpected and hints at a hitherto unexplored area of PK regulation. The enzyme exhibits high specificity for 3PG over other C_3 intermediates of glycolysis, and this metabolic arrangement appears to represent coordinated regulation between PK and GAPOR in the ancestral glycolysis of *P. aerophilum*.

■ ASSOCIATED CONTENT

Supporting Information

Secondary structure assignments of *Pa*PK and multisequence alignment of representative PK sequences (Figure S1), superimposition of the backbones of molecules A and B of the asymmetric unit of the *Pa*PK structure (Figure S2), active site of *Pa*PK with corresponding electron density (Figure S3), structural comparisons of *Pa*PK with other PK structures (Figure S4), comparison of *Pa*PK with *Lm*PK in the T and R states (Figure S5), superimposition of the respective C domains of *Pa*PK and *Lm*PK (Figure S6), and response of *Pa*PK to potential allosteric effectors (Table S1). This material is available free of charge via the Internet at http://pubs.acs.org.

■ AUTHOR INFORMATION

Corresponding Author

*C.D.: Department of Biochemistry and Molecular Biology, Medical University of South Carolina, 173 Ashley Ave., Charleston, South Carolina 29425; telephone, (843) 876-2303; fax, (843) 792-8568; e-mail, davies@musc.edu. P.S.: Institut für Allgemeine Mikrobiologie, Christian-Albrechts Universität Kiel, Am Botanischen Garten 1-9, D-24118 Kiel, Germany; telephone, +49 431-880-4328; fax, +49 431-880-2194; e-mail, peter.schoenheit@ifam.uni-kiel.de.

Present Address

§J.T.G.S.: Department of Microbiology and Immunology, State University of New York at Buffalo, Buffalo, NY 14214.

Author Contributions

J.T.G.S. and U.J. contributed equally to this work.

Notes

The authors declare no competing financial interest.

■ ACKNOWLEDGMENTS

Use of the Advanced Photon Source was supported by the U.S. Department of Energy, Office of Science, Office of Basic Energy Sciences, under Contract W-31-109-ENG-38. Data were collected at the Southeast Regional Collaborative Access

Team (SER-CAT) 22-ID beamline at the Advanced Photon Source. Supporting institutions may be found at http://www.ser-cat.org/members.html. The X-ray crystallography facility used for this work is supported by the Medical University of South Carolina's Research Resource Facilities program. Figures were prepared using MOLSCRIPT[50] and RASTER3D[51] or Pymol (http://pymol.sourceforge.net).

■ ABBREVIATIONS

3PG, 3-phosphoglycerate; FBP, fructose 1,6-bisphosphate; F-2,6-BP, fructose 2,6-bisphosphate; GAPOR, glyceraldehyde 3-phosphate ferredoxin oxidoreductase; GAP, glyceraldehyde 3-phosphate; *Lm*PK, *L. mexicana* pyruvate kinase; *Pa*PK, *P. aerophilum* pyruvate kinase; PDB, Protein Data Bank; PEP, phosphoenolpyruvate; PK, pyruvate kinase; *Sc*PK, *Saccharomyces cerevisiae* (yeast) pyruvate kinase; R5P, ribose 5-phosphate; rmsd, root-mean-square deviation.

■ REFERENCES

(1) Kayne, F. J. (1973) Pyruvate kinase. In *The Enzymes* (Boyer, P. D., Ed.) 3rd ed., pp 353−382, Academic Press, New York.
(2) Kachmar, J. F., and Boyer, P. D. (1953) Kinetic analysis of enzyme reactions. II. The potassium activation and calcium inhibition of pyruvic phosphoferase. *J. Biol. Chem. 200*, 669−682.
(3) Gupta, R. K., and Oesterling, R. M. (1976) Dual divalent cation requirement for activation of pyruvate kinase; essential roles of both enzyme- and nucleotide-bound metal ions. *Biochemistry 15*, 2881−2887.
(4) Mesecar, A. D., and Nowak, T. (1997) Metal-ion-mediated allosteric triggering of yeast pyruvate kinase. 1. A multidimensional kinetic linked-function analysis. *Biochemistry 36*, 6792−6802.
(5) Hall, E. R., and Cottam, G. L. (1978) Isozymes of pyruvate kinase in vertebrates: Their physical, chemical, kinetic and immunological properties. *Int. J. Biochem. 9*, 785−793.
(6) Hess, B., Haeckel, R., and Brand, K. (1966) FDP-activation of yeast pyruvate kinase. *Biochem. Biophys. Res. Commun. 24*, 824−831.
(7) Waygood, E. B., and Sanwal, B. D. (1974) The control of pyruvate kinases of *Escherichia coli*. I. Physicochemical and regulatory properties of the enzyme activated by fructose 1,6-diphosphate. *J. Biol. Chem. 249*, 265−274.
(8) Waygood, E. B., Rayman, M. K., and Sanwal, B. D. (1975) The control of pyruvate kinases of *Escherichia coli*. II. Effectors and regulatory properties of the enzyme activated by ribose 5-phosphate. *Can. J. Biochem. 53*, 444−454.
(9) van Schaftingen, E., Opperdoes, F. R., and Hers, H. G. (1985) Stimulation of *Trypanosoma brucei* pyruvate kinase by fructose 2,6-bisphosphate. *Eur. J. Biochem. 153*, 403−406.
(10) Sakai, H., Suzuki, K., and Imahori, K. (1986) Purification and properties of pyruvate kinase from *Bacillus stearothermophilus*. *J. Biochem. 99*, 1157−1167.
(11) Garcia-Olalla, C., and Garrido-Pertierra, A. (1987) Purification and kinetic properties of pyruvate kinase isoenzymes of *Salmonella typhimurium*. *Biochem. J. 241*, 573−581.
(12) Bakszt, R., Wernimont, A., Allali-Hassani, A., Mok, M. W., Hills, T., Hui, R., and Pizarro, J. C. (2010) The crystal structure of *Toxoplasma gondii* pyruvate kinase 1. *PLoS One 5*, e12736.
(13) Jurica, M. S., Mesecar, A., Heath, P. J., Shi, W., Nowak, T., and Stoddard, B. L. (1998) The allosteric regulation of pyruvate kinase by fructose-1,6-bisphosphate. *Structure 6*, 195−210.
(14) Morgan, H. P., McNae, I. W., Nowicki, M. W., Hannaert, V., Michels, P. A., Fothergill-Gilmore, L. A., and Walkinshaw, M. D. (2010) Allosteric mechanism of pyruvate kinase from *Leishmania mexicana* uses a rock and lock model. *J. Biol. Chem. 285*, 12892−12898.
(15) Jetten, M. S., Gubler, M. E., Lee, S. H., and Sinskey, A. J. (1994) Structural and functional analysis of pyruvate kinase from *Corynebacterium glutamicum*. *Appl. Environ. Microbiol. 60*, 2501−2507.
(16) Johnsen, U., Hansen, T., and Schönheit, P. (2003) Comparative analysis of pyruvate kinases from the hyperthermophilic archaea *Archaeoglobus fulgidus*, *Aeropyrum pernix*, and *Pyrobaculum aerophilum* and the hyperthermophilic bacterium *Thermotoga maritima*: Unusual regulatory properties in hyperthermophilic archaea. *J. Biol. Chem. 278*, 25417−25427.
(17) Noguchi, T., Inoue, H., and Tanaka, T. (1986) The M1- and M2-type isozymes of rat pyruvate kinase are produced from the same gene by alternative RNA splicing. *J. Biol. Chem. 261*, 13807−13812.
(18) Noguchi, T., Yamada, K., Inoue, H., Matsuda, T., and Tanaka, T. (1987) The L- and R-type isozymes of rat pyruvate kinase are produced from a single gene by use of different promoters. *J. Biol. Chem. 262*, 14366−14371.
(19) Christofk, H. R., Vander Heiden, M. G., Harris, M. H., Ramanathan, A., Gerszten, R. E., Wei, R., Fleming, M. D., Schreiber, S. L., and Cantley, L. C. (2008) The M2 splice isoform of pyruvate kinase is important for cancer metabolism and tumour growth. *Nature 452*, 230−233.
(20) Ikeda, Y., Tanaka, T., and Noguchi, T. (1997) Conversion of non-allosteric pyruvate kinase isozyme into an allosteric enzyme by a single amino acid substitution. *J. Biol. Chem. 272*, 20495−20501.
(21) El-Maghrabi, M. R., Claus, T. H., McGrane, M. M., and Pilkis, S. J. (1982) Influence of phosphorylation on the interaction of effectors with rat liver pyruvate kinase. *J. Biol. Chem. 257*, 233−240.
(22) Stetter, K. O. (2006) Hyperthermophiles in the history of life. *Philos. Trans. R. Soc., B 361*, 1837−1842.
(23) Völkl, P., Huber, R., Drobner, E., Rachel, R., Burggraf, S., Trincone, A., and Stetter, K. O. (1993) *Pyrobaculum aerophilum* sp. nov., a novel nitrate-reducing hyperthermophilic archaeum. *Appl. Environ. Microbiol. 59*, 2918−2926.
(24) Siebers, B., and Schönheit, P. (2005) Unusual pathways and enzymes of central carbohydrate metabolism in Archaea. *Curr. Opin. Microbiol. 8*, 695−705.
(25) Reher, M., Gebhard, S., and Schonheit, P. (2007) Glyceraldehyde-3-phosphate ferredoxin oxidoreductase (GAPOR) and nonphosphorylating glyceraldehyde-3-phosphate dehydrogenase (GAPN), key enzymes of the respective modified Embden-Meyerhof pathways in the hyperthermophilic crenarchaeota *Pyrobaculum aerophilum* and *Aeropyrum pernix*. *FEMS Microbiol. Lett. 273*, 196−205.
(26) Schramm, A., Siebers, B., Tjaden, B., Brinkmann, H., and Hensel, R. (2000) Pyruvate kinase of the hyperthermophilic crenarchaeote *Thermoproteus tenax*: Physiological role and phylogenetic aspects. *J. Bacteriol. 182*, 2001−2009.
(27) Valentini, G., Mattevi, A., Barilla, D., Galizzi, A., and Speranza, M. L. (1997) Recombinant pyruvate kinase type I from *Escherichia coli*: Overproduction and revised C-terminus of the polypeptide. *Biol. Chem. 378*, 719−721.
(28) Otwinowski, Z., and Minor, W. (1997) Processing of X-ray diffraction data collected in oscillation mode. In *Methods in Enzymology, Macromolecular Crystallography, Part A*, pp 307−326, Academic Press, Inc., New York.
(29) Vagin, A., and Teplyakov, A. (1997) MOLREP: An automated program for molecular replacement. *J. Appl. Crystallogr. 30*, 1022−1025.
(30) Rigden, D. J., Phillips, S. E., Michels, P. A., and Fothergill-Gilmore, L. A. (1999) The structure of pyruvate kinase from *Leishmania mexicana* reveals details of the allosteric transition and unusual effector specificity. *J. Mol. Biol. 291*, 615−635.
(31) Jones, T. A., Zou, J.-Y., Cowtan, S. W., and Kjeldgaard, M. (1991) Improved methods for building protein structures in electron-density maps and the location of errors in these models. *Acta Crystallogr. A47*, 110−119.
(32) Murshudov, G. N., Vagin, A. A., and Dodson, E. J. (1997) Refinement of macromolecular structures by the maximum-likelihood method. *Acta Crystallogr. D53*, 240−255.
(33) Laskowski, R. A., MacArthur, M. W., Moss, D. S., and Thornton, J. M. (1993) PROCHECK: A program to check the stereochemical quality of protein structures. *J. Appl. Crystallogr. 26*, 283−291.

(34) Stuart, D. I., Levine, M., Muirhead, H., and Stammers, D. K. (1979) Crystal structure of cat muscle pyruvate kinase at a resolution of 2.6 Å. *J. Mol. Biol. 134*, 109−142.
(35) Muirhead, H., Clayden, D. A., Barford, D., Lorimer, C. G., Fothergill-Gilmore, L. A., Schiltz, E., and Schmitt, W. (1986) The structure of cat muscle pyruvate kinase. *EMBO J. 5*, 475−481.
(36) Larsen, T. M., Laughlin, L. T., Holden, H. M., Rayment, I., and Reed, G. H. (1994) Structure of rabbit muscle pyruvate kinase complexed with Mn^{2+}, K^+, and pyruvate. *Biochemistry 33*, 6301−6309.
(37) Mattevi, A., Valentini, G., Rizzi, M., Speranza, M. L., Bolognesi, M., and Coda, A. (1995) Crystal structure of *Escherichia coli* pyruvate kinase type I: Molecular basis of the allosteric transition. *Structure 3*, 729−741.
(38) Valentini, G., Chiarelli, L. R., Fortin, R., Dolzan, M., Galizzi, A., Abraham, D. J., Wang, C., Bianchi, P., Zanella, A., and Mattevi, A. (2002) Structure and function of human erythrocyte pyruvate kinase. Molecular basis of nonspherocytic hemolytic anemia. *J. Biol. Chem. 277*, 23807−23814.
(39) Dombrauckas, J. D., Santarsiero, B. D., and Mesecar, A. D. (2005) Structural basis for tumor pyruvate kinase M2 allosteric regulation and catalysis. *Biochemistry 44*, 9417−9429.
(40) Larsen, T. M., Benning, M. M., Rayment, I., and Reed, G. H. (1998) Structure of the bis(Mg^{2+})-ATP-oxalate complex of the rabbit muscle pyruvate kinase at 2.1 Å resolution: ATP binding over a barrel. *Biochemistry 37*, 6247−6255.
(41) Oria-Hernandez, J., Cabrera, N., Perez-Montfort, R., and Ramirez-Silva, L. (2005) Pyruvate kinase revisited: The activating effect of K^+. *J. Biol. Chem. 280*, 37924−37929.
(42) Laughlin, L. T., and Reed, G. H. (1997) The monovalent cation requirement of rabbit muscle pyruvate kinase is eliminated by substitution of lysine for glutamate 117. *Arch. Biochem. Biophys. 348*, 262−267.
(43) Oria-Hernandez, J., Riveros-Rosas, H., and Ramirez-Silva, L. (2006) Dichotomic phylogenetic tree of the pyruvate kinase family: K^+-dependent and -independent enzymes. *J. Biol. Chem. 281*, 30717−30724.
(44) Fenton, A. W., and Blair, J. B. (2002) Kinetic and allosteric consequences of mutations in the subunit and domain interfaces and the allosteric site of yeast pyruvate kinase. *Arch. Biochem. Biophys. 397*, 28−39.
(45) Cheng, X., Friesen, R. H., and Lee, J. C. (1996) Effects of conserved residues on the regulation of rabbit muscle pyruvate kinase. *J. Biol. Chem. 271*, 6313−6321.
(46) Friesen, R. H., and Lee, J. C. (1998) The negative dominant effects of T340M mutation on mammalian pyruvate kinase. *J. Biol. Chem. 273*, 14772−14779.
(47) Cook, W. J., Senkovich, O., Aleem, K., and Chattopadhyay, D. (2012) Crystal structure of *Cryptosporidium parvum* pyruvate kinase. *PLoS One 7*, e46875.
(48) Denton, H., Brown, S. M., Roberts, C. W., Alexander, J., McDonald, V., Thong, K. W., and Coombs, G. H. (1996) Comparison of the phosphofructokinase and pyruvate kinase activities of *Cryptosporidium parvum*, *Eimeria tenella* and *Toxoplasma gondii*. *Mol. Biochem. Parasitol. 76*, 23−29.
(49) Say, R. F., and Fuchs, G. (2010) Fructose 1,6-bisphosphate aldolase/phosphatase may be an ancestral gluconeogenic enzyme. *Nature 464*, 1077−1081.
(50) Kraulis, P. J. (1991) MOLSCRIPT: A program to produce both detailed and schematic plots of protein structures. *J. Appl. Crystallogr. 24*, 946−950.
(51) Merritt, E. A., and Murphy, M. E. P. (1994) Raster3D version 2.0. A program for photorealistic molecular graphics. *Acta Crystallogr. D50*, 869−873.
(52) Tulloch, L. B., Morgan, H. P., Hannaert, V., Michels, P. A., Fothergill-Gilmore, L. A., and Walkinshaw, M. D. (2008) Sulphate removal induces a major conformational change in *Leishmania mexicana* pyruvate kinase in the crystalline state. *J. Mol. Biol. 383*, 615−626.